TECHNISCHE UNIVERSITÄT WIEN

institute of telecommunications

VIENNA SCIENTIFIC CLUSTER

*DIPLOMA THESIS*

# *Estimation of electromagnetic conductivity in seawater based on acoustic propagation characteristics*

*To obtain the academic degree of*

*Dipl. engineer*

*As part of the academic program*

*Master programme Embedded Systems*

*submitted by*

*Melic Alena*
*Matriculation Number 01125426*

*Performed at the Institute of Telecommunications*
*of the Faculty of Electrical Engineering at Vienna University of Technology*
*in collaboration with the Vienna Scientific Cluster*

*Supervision*
*Supervisor: Univ.Prof. Ing. Dipl.-Ing. Dr.-Ing.Christoph Mecklenbräuker*
*Co- Supervisor: PHD John Fenton*

## *Affidavit*

I declare in lieu of oath, that I wrote this thesis and carried out the associated research myself, using only the literature cited in this volume. If text passages from sources are used literally, they are marked as such.

I confirm that this work is original and has not been submitted for examination elsewhere, nor is it currently under consideration for a thesis elsewhere.

I acknowledge that the submitted work will be checked electronically-technically using suitable and state-of-the-art means (plagiarism detection software). On the one hand, this ensures that the submitted work was prepared according to the high-quality standards within the applicable rules to ensure good scientific practice "Code of Conduct" at the TU Wien. On the other hand, a comparison with other student theses avoids violations of my personal copyright.

| | |
|---|---|
| *Place and Date* | *Signature* |

## Abstract

Most underwater communication and sensing systems use acoustic waves. However, acoustic signals cause stress to animals. Transmission systems with lasers are limited by turbidity. The use of electromagnetic waves presents a possible interesting alternative, however the penetration depth of electromagnetic waves under water is limited due to physical properties. In this work, the aim is to infer the specific conductance based on measurements of salinity and temperature, and by the waves arriving at the shore generated by the wind over a wide range; accurate estimates of the specific conductance, especially if they are low, may lead to increased use of electromagnetic/ optic communication systems underwater.

## Kurzfassung

Die meisten Unterwasserkommunikations- und -erkennungssysteme nutzen akustische Wellen. Akustische Signale verursachen jedoch Stress bei den Tieren. Übertragungssysteme mit Lasern werden durch Trübungen eingeschränkt. Die Eindringtiefe elektromagnetischer Wellen unter Wasser wird durch physikalische Eigenschaften begrenzt, vor allem durch den spezifischen Leitwert. Ziel dieser Arbeit ist es, den spezifischen Leitwert auf der Grundlage von Messungen des Salzgehalts und der Temperatur sowie der an der Küste eintreffenden, durch den Wind erzeugten Wellen in einem weiten Bereich zu bestimmen; genaue Schätzungen des spezifischen Leitwerts, insbesondere wenn sie niedrig sind, können zu einer verstärkten Nutzung elektromagnetischer/ optischer Kommunikationssysteme unter Wasser führen.

## Acknowledgements

The first thank goes to all those who made it possible for me to have a lot of fun in this subject area. They showed me that when it comes down to it, one only needs paper, pen, and determination (if paper and pen are even necessary) to comprehend.

I would like to express my gratitude to Univ.Prof. Ing. Dipl.-Ing. Dr.-Ing. Mecklenbräuker Christoph and Dr John Fenton for supervising my thesis and the course wave propagation. This course has inspired following thoughts: "Waves are waves, regardless of the medium or type", "Directional characteristics are present not only in electromagnetic propagation, but also in light and sound!" and "The length of a submarine- antenna...".

I would like to extend my special thanks to former hydroacoustician Dipl. Ing. Mark Meise for providing me with valuable books (e.g. Atlas Electronics, ...) and for his encouragement: "If you understand the formulas of hydroacoustics, then pursue hydroacoustics!" and "Knowledge is not something to be feared! Embrace it! “have been truly motivating.

Finally, I would like to thank the Vienna Scientific Cluster and its dedicated team for their invaluable support in providing computing resources.

# Contents

# Introduction

*"If you want to build a ship, don't drum up the men to gather wood, divide the work and give orders. Instead, teach them to yearn for the vast and endless sea."- Antoine de Saint-Exupéry*

This thesis represents a significant section of my research focussing on the interplay of electromagnetic and acoustic waves. As we are aware most underwater communication and sensing systems use acoustic waves due to the low loss propagation. However, this type of signal transmission is prone to interference. The idea of my research is to combine acoustic and electromagnetic/ optic transmission, to enhance the accuracy of signal transmission (joint propagation of sensor array data).

Most underwater communication systems rely on acoustics, as acoustic waves are better suited for propagation in water. However, this type of wave propagation is susceptible to interference, which can pose challenges for communication, particularly in situations requiring distress signals, such as submarines. For instance, in the case to locate a submerged submarine, one can exploit the fact that it is constructed of metal. A sonar system emits sound beams into the water, which travel approximately five times faster than in air. These beams are deflected by the submarine and captured as an image on a technical display. However, water represents a significant challenge due to its nonhomogeneous nature. It consists of various layers with differing temperatures and salinity levels, which are subject to constant change. The presence of such layers can cause the sound beam to be deflected, making it difficult to locate the object beneath. The primary objective of this thesis is to gain better understanding of these layers by analysing acoustic measurement data and by comparing to corresponding mathematical models.

- As previously mentioned, the properties of water, such as salinity (S), density, turbidity, and temperature (T) are not uniform and vary in distinct layers. These factors interact with each other, affecting the speed of sound. The values of salinity, density, turbidity, depth(z) and temperature influence each other. The determination of sound velocity values, for example can be obtained by:

$$v = 1449.2 + 4.6\,T - 0.055\,T^2 + 0.00029\,T^3 + (1.34 - 0.01\,T)\,(S - 35) + 0.016\,z \quad (1)$$

*(F.B. Jensen, 1994)*

Another parameter that undergoes changes is the electromagnetic conductivity, primarily influenced by salinity. The measurement of salinity is dependent on factors like temperature, altitude, and the speed of sound. Furthermore, an additional objective of this research is to gain insights into salinity values and consequently, the electromagnetic conductivity through acoustic measurement data from a hydrophone array near the island of Elba. Typically, salinity values are determined using electromagnetic conductivity. In this work, a regression should take place. The aim is to derive the conductivity profile based on the determined salinity values, particularly within the range of up to 100 meters of water depth. This depth range is crucial, as it provides a starting point for an acoustic receiver, which receives acoustic data (sound speed) from waves near the shore. Therefore, it is recommended to calculate for a profile of approximately 100- meter depth (typical diving depth of conventional submarines).

- The penetration depth of electromagnetic waves is explained by this simple formula:

$$\delta = \sqrt{\frac{2}{\omega\mu\sigma}} \quad (2)$$

where $\delta$ is the penetration depth, $\omega$ is the angular frequency, $\sigma$ is the electromagnetic conductivity, and $\mu$ is the permeability. By applying this formula to calculate the penetration depth of

electromagnetic waves in the atmosphere and consequently the range, it becomes evident, that at a frequency up to 2 GHz (such as WLAN), the penetration depth spans several meters. However, in a medium like water, it is limited to only a few centimetres. Gaining more knowledge about the electromagnetic conductivity in water can facilitate greater propagation of electromagnetic waves in this medium, despite its high attenuation value.

## Modelling and measuring acoustic and electromagnetic propagation media characteristics

To assess parameters such as sound speed and density and conductivity in seawater, as well as simulate a model, a diverse range of sensors and approximation methods can be employed. This section will provide descriptions of some of these methods.

### Modelling key acoustic propagation media characteristics

Key acoustic media characteristics are sound speed and density profiles, whereas permittivity and conductivity are key characteristics for electromagnetic propagation. The modelling process for both is similar, the nature of the waves differs (transverse waves for electromagnetic propagation and longitudinal waves for acoustic propagation). The Helmholtz equation serves for both as a foundation and can be solved either numerically or analytically.

#### *Simple sound propagation model*

- Sound propagation in gases and liquids is described by spatial fluctuations around a rest position, which affect the physical quantities pressure, density, and velocity of the particles:

$$p = p_0 + p_\sim \quad (3)$$

$$\rho = \rho_0 + \rho_\sim \quad (4)$$

$$v = v_0 + v_\sim \quad (5)$$

- By the total differential of the velocity vector for a volume element (The first term is the change of the velocity field with time, the second considers that the element moves to a different location due to the motion):

$$dV = \partial_t v \, dt + (dr \,.\nabla)v \quad (6)$$

one can see how pressure and sound velocity influence each other (the acceleration must be expressed by force; gravity and viscosity were neglected to find a simple solution; density is considered constant)

$$\rho \, \partial_t v \; + \; (v \,.\nabla)v = -\nabla \mathrm{p} \quad (7)$$

- If it is assumed that the plane wave is valid only in one direction (in $x$) in the sound propagation, then the equation can be simplified for one direction, and the solution for pressure is

$$p_\sim = p_1 f\left(t \mp \frac{x}{c}\right) \quad (8)$$

with the characteristic impedance

$$Z_0 = \frac{p_\sim}{v_\sim} \quad (9)$$

and for water the characteristic impedance is

$$Z_0 = \; 1.5 \; 10^6 \; Pa \; s \quad (10)$$

In sound propagation, there is friction (caused by dynamic viscosity), thermal conductivity (compression and pressure variations cause temperature changes), and molecular absorption. These are all attenuation factors that can be included to determine the sound velocity in a model. In addition to attenuation factors, bottom loss and volume scattering could appear and modify the solution.

*Helmholtz Equation*

- The wave equation for pressure with constant density is:

$$\nabla^2 p - \frac{1}{c^2}\frac{\partial^2 p}{\partial t^2} = 0 \quad (11)$$

  whereas c is the speed of sound.

- The wave equation for displacement potential is:

$$\nabla^2 \Phi - \frac{1}{c^2}\frac{\partial^2 \Phi}{\partial t^2} = 0 \quad (12)$$

  whereas the kinematic relation between velocity and displacement $v = \dot{u}$. The displacement potential is defined by $u = \nabla\Phi$. Discrete changes in density are handled by appropriate boundary conditions between regions of constant density. The boundary conditions require then continuity of pressure and displacement. Therefore, the acoustic pressure in terms of the displacement potential is defined by:

$$p = -\rho c^2 \nabla^2 \Phi \quad (13)$$

The underwater acoustic pressure signals can be modelled using a variety of methods, enabling us to gain a certain level of understanding trough their analysis:

- Ray- Methods (used to explain sound propagation in water, but should not be chosen for higher-value applications)
- Wavenumber Integration Techniques
- Normal Modes Methods
- Parabolic Equation
  - Standard Parabolic Equation
  - Generalized Parabolic Equation
  - Elastic Parabolic Equation

  The Split Step Fourier Algorithm

  Since many practical ocean acoustics problems are narrow angle problems with little to no bottom interaction, the split step technique will remain the preferred technique for sonar-performance. The Split Step algorithm is used to solve the standard PE.

The principal advantage of the various parabolic wave equations is that they can be solved by split-step- Fourier technique and various FE and FD techniques. This technique is computationally efficient for long range, narrow angle propagation. For short-range, deep-water problems and shallow water problems in general, this requires wide- angled PEs, which can be solved by FD.

- Finite Differences Methods
- Finite Elements Methods
- etc.

(F.B. Jensen, 1994)

*Normal Mode Method vs. Finite Element Method*

In this section we compare the results of a model of the sound pressure field in response to an isotropic point source emitting a sinusoidal spherical wave in shallow ocean, approximated by the normal mode method and the finite element method.

## Normal Mode Method

Normal mode methods and boundary element methods have drawbacks, as they provide solutions and estimations either fully determined in two dimensions (2D) or within a specific range in 2D).

## Normal Mode Method- Formulation

- In underwater acoustics, it is customary to consider a medium in which density ρ and the velocity c depend on the depth coordinate z. Later a weak horizontal variation can be approximately accounted for using adiabatic approximation. The motivation behind this method lies in the Hankel transformation for the sought- after Green's function:

$$G(r, r_0, \omega) = \frac{-j}{4\rho(z_0)} \sum_{\alpha=1}^{A(\omega)} \varphi_\alpha(z)\varphi_\alpha(z_0) H_0^{(2)}(k_\alpha R) - \int_{C_{BJP}} . \quad (14)$$

The subsequent figure illustrates the sound pressure field in response to an isotropic point source emitting a sinusoidal spherical wave of 250 Hz estimated by the normal mode method:

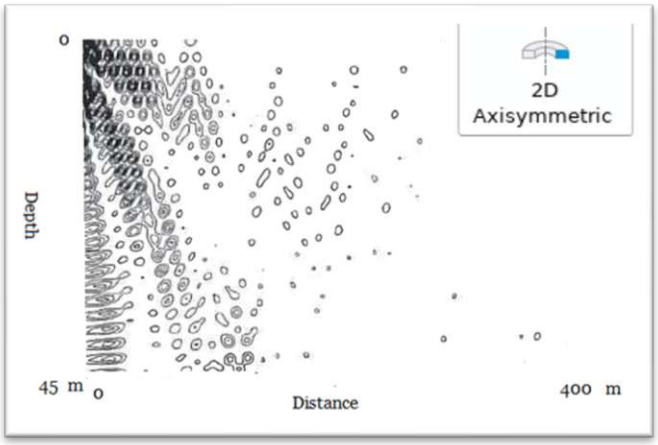


*Figure 1: Analytical Solution for the Sound pressure field: Normal Mode Method*

A small calculation error arises from the omission of the integral term from the equation in the program implementation (Mecklenbräuker, 1998).

## Finite Element Method

Finite element and finite differences solver are usually used for finite volume calculations, a problem with the ocean. Through specific boundary conditions such as the perfectly matched layer (PML) calculations and approximations are nevertheless achievable. The PML setup allows one or two modes with a specific wave number to pass the modelling domain with minimal reflections. We specified the size of the modelling domain to be 130 meters in width ties 130 meters in depth times 130 meters in height.

- The sea surface is simulated by the Dirlichlet Boundary:

$$p = 0 \quad (15)$$

- The seabed is simulated by the Neumann Boundary:

$$\frac{dp}{dn} = 0 \quad (16)$$

We dealt with the open boundaries with the PML setup. One limitation of this method is its high computational cost in comparison to the normal mode method. Advantages, however, are: Its ease and speed of application, allowing for easy modification of the parameters being modelled and their interdependencies. For example, it enables the inclusion of scattering, ocean damping and perturbation effects.

### Finite Element Method- Formulation

Let Ψ be a function space generated by functions Φ(x) that are sufficiently often differentiable with compact supports. The elements ϕ(x) of this generating system are called test functions. For example, let $u_x(x, t) = f(x)$.

- First, choose Ψ as any space with at least one continuously differentiable function ϕ(x) with bounded support.

$$u_x(\mathrm{x},\mathrm{t})\Phi(\mathrm{x}) = \mathrm{f}(\mathrm{x})\Phi(\mathrm{x}) \quad (17)$$

- Integrate:

$$\int_{-\infty}^{\infty} u_x(\mathrm{x},\mathrm{t})\Phi(\mathrm{x})\mathrm{dx} = \int_{-\infty}^{\infty} \mathrm{f}(\mathrm{x})\Phi(\mathrm{x}) \quad (18)$$

- Partial integration:

$$\int_{-\infty}^{\infty} u_x(\mathrm{x},\mathrm{t})\Phi(\mathrm{x})\mathrm{dx} = [u(t,x)\Phi(x)]_{-\infty}^{\infty} - \int_{-\infty}^{\infty} \mathrm{u}(\mathrm{t},\mathrm{x})\Phi_x(\mathrm{x})\mathrm{dx} = -\int_{-\infty}^{\infty} \mathrm{u}(\mathrm{t},\mathrm{x})\Phi_x(\mathrm{x})\mathrm{dx} \quad (19)$$

The gray-highlighted part of the partial integration is the compact support and must vanish.

From the strong formulation:

$$u_x(\mathrm{x},\mathrm{t})\Phi(\mathrm{x}) = \mathrm{f}(\mathrm{x})\Phi(\mathrm{x}) \quad (20)$$

we derive the weak formulation:

$$-\int_{-\infty}^{\infty} \mathrm{u}(\mathrm{t},\mathrm{x})\Phi_x(\mathrm{x})\mathrm{dx} = \int_{-\infty}^{\infty} \mathrm{f}(\mathrm{x})\Phi(\mathrm{x})\mathrm{dx} \quad (21)$$

u(t, x) does not need to be differentiable everywhere anymore.

The finite object to be integrated is partitioned into triangles/tetrahedra, each transformed into what are known as 'hat functions,' with each of these functions being assigned its corresponding physical interpretation and conditions.

### *Finite Element Method- Formulation for Acoustics*

1. The acoustic domain is divided by a mesh of finite elements, the equation that needs to be solved for each element with their specific boundary conditions e.g.:

$$\nabla \cdot \left(-\frac{1}{\varrho_c}(\nabla p_t - q_d)\right) - \frac{k_{eq}^2\, p_t}{\varrho_c} = Q_m \quad (22)$$

$$k_{eq}^2 = \left(\frac{\omega}{c_c}\right)^2 \quad (23)$$

2. The choice and arrangement of these elements depend on the specific problem being solved. We specified the maximum tolerable element size to be:

$$\frac{\lambda}{5} \quad (25)$$

3. The acoustic wave equation is formulated in terms of the unknown acoustic pressure field. This equation is derived by the physical properties of the medium.

4. The local equations are combined to form a global system of equations that represents the entire domain.

5. The global system of equations is solved numerically at each node.

$$(K_a - \Lambda_n^2 M_a)\Phi_n = 0 \quad (26)$$

$$K_a = \int_V B_a^T B_a dV \quad (27)$$

$$M_a = \int_V \frac{1}{C_0^2} N_a^T N_a dV \quad (28)$$

$$B_a = [d/dx, d/dy, d/dz]^T N_a \quad (29)$$

In following figures, the sound pressure field is estimated from a point source emitting a sinusoidal spherical wave (170 Hz). Additionally, in this case the point source is located at a depth of 65 meters, which roughly corresponds to the experiment presented later in this thesis:

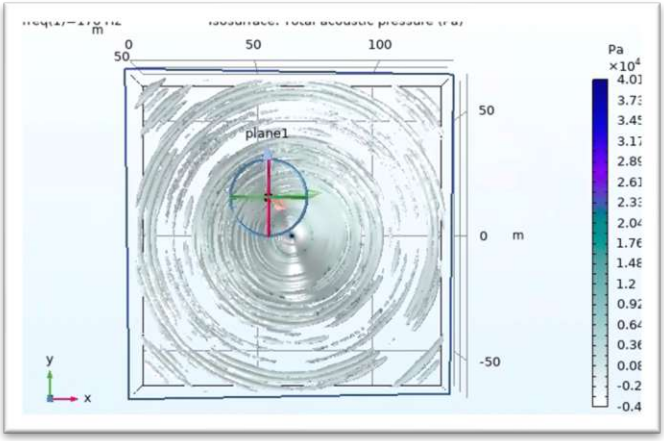


*Figure 2: Numerical Solution for the Sound pressure field: Finite Element Method x-, y- axis*

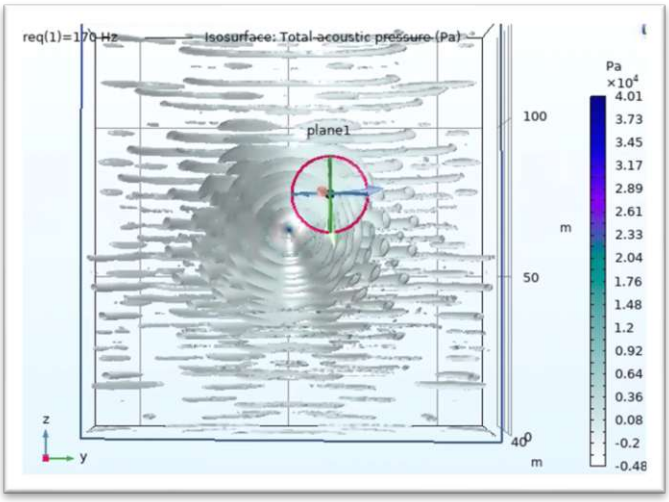


*Figure 3: Numerical Solution for the Sound pressure field: Finite Element Method y-, z- axis*

As computer performance continues to improve, the finite element method is recommended for further model validations. It allows the incorporation of element- wise scattering disturbances, attenuation factors and acoustic flow source coupling. More suitable model approximations are achievable.

## Modelling electromagnetic propagation media characteristics

The finite element method has demonstrated its effectiveness as a versatile numerical modelling technique. Its successful application in approximating the acoustic pressure field in shallow oceans is indicative of its potential to yield promising results in other respective fields, such as the electromagnetic field, for e.g., obtaining the power density. While the modelling process for electromagnetic and acoustic waves shares similarities (the Helmholtz equation serves for both as a foundation and can be solved either analytically or numerically), it's important to note that the nature of these waves differs, with electromagnetic waves being transverse and acoustic waves being longitudinal.

### *Electromagnetic vector potential*

The electromagnetic vector potential is used in electrodynamics to describe electromagnetic fields and wave propagation in electromagnetic systems. It is closely related to the magnetic field (B- field), the electric potential, it provides an alternative representation of the Maxwell's equations and can therefore be used to infer power density properties.

- The Maxwell equations are:

$$\nabla \cdot D = \rho \quad (30)$$

$$\nabla \cdot B = 0 \quad (31)$$

$$\nabla \times E = -\frac{\partial}{\partial t} B \quad (32)$$

$$\nabla \times H = J_e + \frac{\partial}{\partial t} D \quad (33)$$

The last two equations are Faraday's law of electromagnetic induction and Ampère's Maxwell's law.

- We consider a pure vortex field in advance harmonic processes:

$$B = \nabla \times A \quad (34)$$

$$H = \frac{1}{\mu} \nabla \times A \quad (35)$$

and insert this equation in Faradays law of electromagnetic induction:

$$\nabla \times E = -j\omega \nabla \times A \quad (36)$$

$$\nabla \times (E + j\omega A) = 0 \quad (37)$$

- For the electric field, it would then apply:

$$E + j\omega A = -\nabla \phi \quad (38)$$

$$E = -j\omega A - \nabla \phi \quad (39)$$

which is only possible with a scalar potential $\phi$.

- Using these equations and the Lorentz gauge (The choice of a particular gauge, including the Lorentz gauge, depends on the requirements and convenience of a specific problem. In the Lorentz gauge, the divergence of the vector potential is set to vanish with respect to the scalar potential and the speed of light in a vacuum. This simplifies the mathematical treatment of electromagnetic fields and waves in certain special cases.), we've expressed our electric field E and magnetic field H as functions of two potentials, and we can place them into the Ampère-Maxwell's law:

$$\nabla^2 A + \omega^2 \varepsilon \mu A = -\mu J_e \quad (40)$$

- The solution to this equation can be represented as a convolution integral:

$$A(r) = \mu \int_{V'} \frac{J_e(r') e^{-jk|r-r'|}}{4\,\pi |r - r'|} dV' \quad (41)$$

where V' is the source region, r is the incident point, and r' is the observation point of the object.

## Far field approximation

- In the derivation, we consider that the source region is approximately at a distance of r-r' from r, and then, through a cosine approximation, the solution for the electromagnetic potential A will appear differently:

$$A(r) = \mu \frac{e^{-jkr}}{4\pi r} \int_{V'} J_e e^{jkr' cos\phi} dV \quad (42)$$

with parts of the solution as a spherical wave, as a radiation vector and as a complex weighted Fourier Integral. With the far-field approximation, we assert the modelling of an electromagnetic wave emitted from an antenna; it corresponds to a spherical wave. By employing far-field approximations of the electromagnetic potential A, one can infer properties of the electric and magnetic fields E and H.

- Using the equation of the Poynting vector:

$$S = E \times H \quad (43)$$

conclusions can be drawn additionally regarding the power density.

*Note:* Validating the modelling of an antenna by using measurement data; the antenna's properties must be experimentally verified: Typically, this involves measuring received power density and, in some cases, incorporating a reference antenna. Characteristics such as directional pattern and gain are measured and then cross-referenced e.g., with an existing model.

### *Model Setup- Electromagnetic Field*

Given the high electromagnetic conductivity of saltwater, underwater communication using electromagnetic waves often requires a substantial transmitting station to penetrate depths of several hundred meters.

- Naval Radio Station Rhauderfehn- an example

  An example of such a large transmitting station is the Naval Radio Station Rhauderfehn, a longwave transmitter, featuring eight towers, each 352 meters in height, for a total height of 2,816 meters. Each of the eight towers is operated at 20,000 volts (eight times 20 kV approximately 160 kV). All eight towers are equipped with 100-kilowatt transmitters (eight times 100kW approximately 800kW).


*Figure 4: location map*

*Figure 5: transmission station 2004*

Lower frequencies, typically within the range of a few Hertz, are commonly selected for transmission purposes.

Simulating such transmitting stations is approached by using a monopole antenna configuration, characterized by its significant height and capacitive top hat design. Conductivity values are pre-set to observe (e.g.: from 6 S/m to 3 S/m (standard values in shallow ocean)) how the electric field behaves under different conductive conditions in sea water.

- These conductivity values are approximations for values at the surface of the Mediterranean, with conductivity decreasing as depth decreases (Given the observed decrease with CTD measurements in velocity with decreased depth and assuming a corresponding decrease in conductivity, see equation 1).
- To simulate transmitting stations like the Naval Radio Station Rhauderfehn, we consider a monopole- antenna ($\lambda/4$ =2000m, f=34747Hz, U=160kV and Z= 3200$\Omega$) with capacitive top hat, surrounded by a sphere. Half of the sphere consists of air with its electromagnetic propagation characteristics, and the other half consists of saltwater with its respective characteristics. As mentioned earlier, the Finite Element Method is used in both acoustic and electromagnetic cases to obtain approximations for their respective fields.

- For the electromagnetic field, the following form of the Helmholtz equation is employed and needs to be solved for each element:

$$\nabla \times \frac{1}{\mu_r}(\nabla \times E) - k_0^2\left(\varepsilon_r - \frac{j\sigma}{\omega\varepsilon_0}\right)E = 0 \quad (44)$$

where $\mu_r$ is the electromagnetic permeability, $k_0$ the wavevector, $\varepsilon_r$ the electromagnetic permittivity, $\omega$ the angular frequency.

- No boundary conditions were established for the interface between air and the water. Initially, the numerical field was analysed as if it was located solely in an airspace, and subsequently, adjustments were made to the medium, e.g., changes in conductivity in the lower half, changing the medium.
- It is worth noting that this is a finite volume approach and as such, the perfectly matched layer is also applied. The maximum tolerable element size is:

$$d = \frac{\lambda}{5} \quad (45)$$

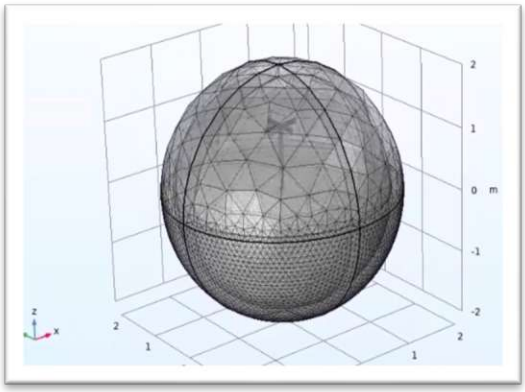

*Figure 6: An example mesh for the FEM for electromagnetic waves, structured as described above. The illustration is provided solely for the purpose of visualizing the antenna and the hat capacity, as well as the division between the medium water and the medium air; for accurate FEM approximations, a finer mesh is required.*

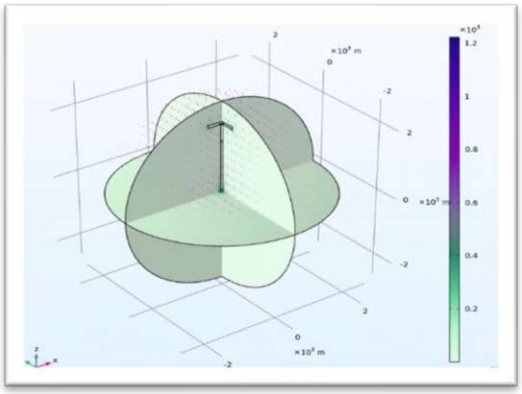

*Figure 7: Result of the FEM Simulation of the monopole antenna configuration with hat capacitance for the electromagnetic field; upper segment air ($\sigma = 0$), lower segment: standard ocean model for conductance: $\sigma = 6$ S/m for the first 30m depth, then $\sigma = 3$ S/m*

We simulate the electromagnetic field response to a monopole antenna emitting a sinusoidal wave at a frequency of 37474 Hz (long-wave range) using the FEM approach.

- We derived a far-field approximation for the electromagnetic field for the electromagnetic potential, see equation 42, we assume that, when examining the approximated values obtained from the FEM method, the far-field approximation criteria should be considered, which is:

$$\frac{2D^2}{\lambda} \leq r \quad (46)$$

In essence, we examine the approximated values at distances greater than this threshold r.

Multiple approximation analyses were conducted: Analysis a) aimed to closely approximate the ocean model, see figure 7, 8 and 9. The results for multiple approximations analyses are depicted in figure 8 and 9. In analysis a) (the orange colour curve (points) in the figures 8 and 9) the electromagnetic

conductivity is pre-set to be as described in the standard ocean model, in analysis, b) (the blue colour curve (points), the electromagnetic conductivity is pre-set to be 6 [S/m] the first 15 m and then 3 [S/m]. Analysis b) is similar to the standard ocean model. The conductivity values from the other analyses are preset to be σ=10 [S/m] (yellow) and σ=0.5 [S/m] (violet). The numerical approximation, based on

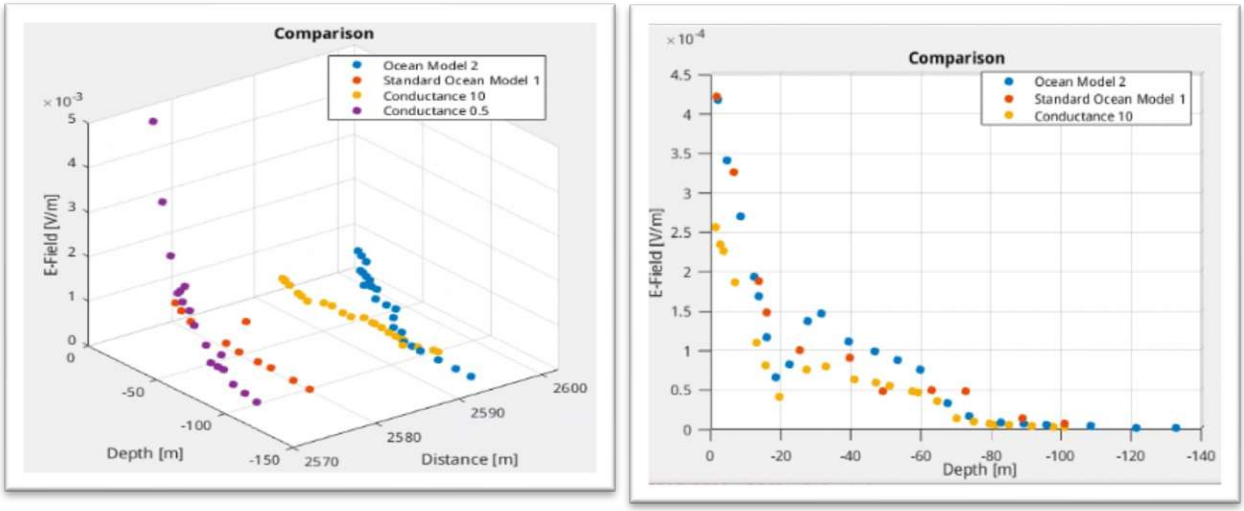


*Figure 8 and 9: FEM Analyses of the electromagnetic field response of an antenna with hat capacitance with different electromagnetic conductivity values for simulating the ocean. Four analyses were conducted, and the values of the electromagnetic field were depicted in the far field.*

estimated conductivity values, indicates that, commencing at a depth of 30 meters, the second ocean model undergoes a transition to 3 [S/m]. At a depth of 15 meters, the conductivity was 6 [S/m]. Preceding this change, similar to ocean model 1 (initially 6 [S/m], transitioning to 3 [S/m] at a depth of 30 meters), it yields improved results for the EM field. However, the noteworthy observation is the inflection point in the curve of ocean model 2. Despite the anticipation of superior EM values from a depth of 15 meters, this inflection suggests that the standard ocean model outperforms up to a depth of approximately 30 meters, see figure 9.

For each case, two APPROXIMATE field strength points were taken, and their distance. From this, the respective attenuation/penetration depth is approximated. Similar values are determined using equation 2. It is important to note that these values were determined for a frequency of 34747 Hz; it is recommended to use a carrier frequency of 15000 Hz for underwater electromagnetic propagation (As a result, the electromagnetic field would be intensified, rendering differences in electromagnetic field strength more discernible and consequently leading to increased penetration depth.).

| **f = 34747Hz** | **Electric field position blue sending position, white receiving position** | **Electric field value blue sending position, white receiving position** | **Penetration depth according to equation 2** |
|---|---|---|---|
| **σ = 0.5 S/m** | -2.407 m | 0.00467268 V/m | 3.81 m |
| | -14.8836 m | 0.0018533 V/m | |
| **σ = σ(Oceanmodel 1)** | -1.17043 m | 0.00418558 V/m | 1.1 m |
| | -24.7538 m | 0.000096645 V/m | |
| **σ = σ(Oceanmodel 2)** | -12.2987 m | 0.000194018 V/m | 1.5588 m |
| | -31.4879 m | 0.00014705 V/m | |
| **σ = 10 S/m** | -1.03414 m | 0.000254446 V/m | 0.85 m |
| | -27.1703 m | 0.0000074 V/m | |

*Table 1: Estimating the penetration/attenuation from numerically approximated electric fields (FEM Analyses)*

Electromagnetic conductivity changes with temperature, pressure, and density.

Numerically it is evident that changes in the electromagnetic field's penetration depth are influenced by variations in conductivity parameters. These changes occur depending on alterations in density, temperature, pressure, and humidity (in simulations and real-world conditions). This implies that under favorable natural conditions, greater penetration depths are achievable, according to the results of the numerical analysis (simulated experiment).

### Measuring key acoustic and electromagnetic propagation media characteristics

The speed of sound in underwater environments is typically around 1485 meters per second (although it can vary due to non- uniformity of water caused by different layers). One of the earliest measurements that closely approximated this value was conducted by Beyer in 1826 in Lake Geneva. In this experiment, a mechanoacoustic transducer was used to generate sound, and the receiver was positioned 13 km away. The measured velocity value, at a temperature of 8°C, was 1438 meters per second. Hydrophones and hydrophone chains are commonly used to determine sound velocity underwater.

One objective of this research is to conduct parameter estimation of velocity and conductivity in underwater environments. Two approaches can be pursued: employing mathematical models and parameter estimation to determine the parameters to a certain extent and then validating them against measured data, or initially conducting measurements and subsequently validating them against one or more models. Furthermore, data can be measured at one point and compared with data obtained at another point in time to obtain a more precise understanding of the properties.

To evaluate parameters such as sound speed, density, electromagnetic conductivity, and salinity in seawater, a diverse range of sensors and approximation methods can be employed. This section will provide descriptions of some of these methods.

#### *Hydrophone*

The hydrophone is considered the most crucial measurement sensor for water sound velocity. It is responsible for converting underwater sound pressure waves (with a measuring range of 10 Hz to 400kHz) into corresponding electrical voltages, preferably utilizing the piezoelectric effect. The sensitivity of a hydrophone, based on the piezoelectric effect, is defined as the ratio between the open circuit voltage amplitude and the free field pressure amplitude of an incident soundwave, often represented by the symbol M. Piezoelectric hydrophone types often provide the logarithmic value of M as a measurement parameter:

$$RVS = 20 \log M \quad (47)$$

For example, PZT-4 plate hydrophone with a thickness of 0.01m, operating in the 33 mode exhibits:

$$RVS = -192dB(V/\mu Pa) \quad (48)$$

(John L. Butler, 2016)

Cylindrical and spherical hydrophones are widely used for measurements due to their design, which offers high sensitivity, a wide-band smooth response up to and potentially through resonance, low impedance, good hydrostatic pressure capability, and simplicity. However, there are also other types available, such as the clay hydrophone mushroom (consisting of parallel wired ceramic sections enclosed in an airfield), the 1-3 Composite hydrophone (manufactured by cubing standard piezoelectric material into a grid, filling the spaces with epoxy resin, and coating both sides for electrical contact), and the Bender hydrophone, among others.

(John L. Butler, 2016)

Hydrophones can be constructed in two ways: A membrane hydrophone is created by stretching a PVDF film over a ring and vapor- depositing it with electrodes. This type of hydrophone offers a high bandwidth with minimal feedback effect on the sound field and is commonly used as a standard hydrophone. Needle hydrophones, on the other hand, have a compact body with a small piezoelectric element attached to the end. They are rougher in design and tend to interfere more with the sound field.

(Koch, 1999)

### *Hydrophone array*

In the context of the "N- Elba Experiment," the measurement data was recorded using a hydrophone array in 1993 in an area with approximately 130 meters water depth. Hydrophone arrays can record data vertically as well horizontally, allowing the analysis of velocity in three axes. In the N- Elba Experiment, the multi- channel hydrophone data was recorded with a vertical antenna (vertical array), low- pass filtered at the antenna, and digitized at a sampling frequency of 1000 Hz. The hydrophone data is transmitted via cable to a radio buoy for further processing.

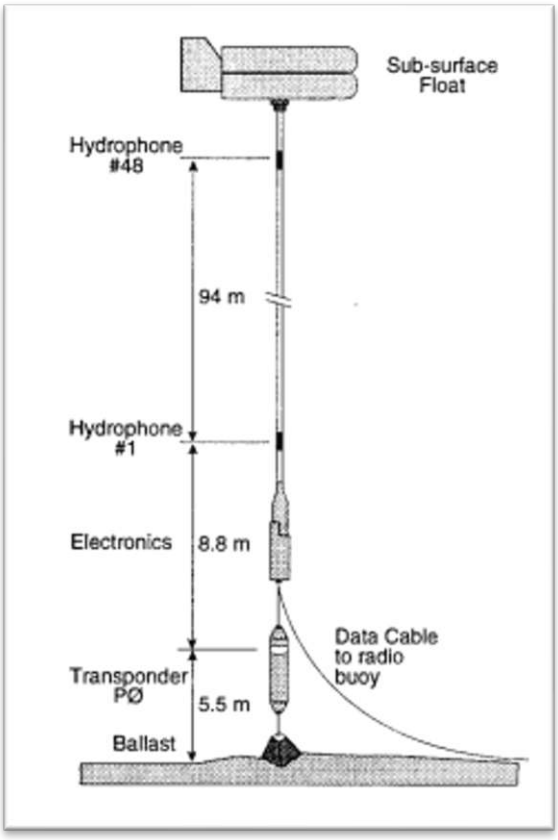


*Figure 10: The SACLANTCEN vertical array*

(Mecklenbräuker, 1998)

### *Sound sources*

For measurements it is advisable to generate a PRN (Pseudo- Random Noise) signal at a specific frequency to ensure reliable detection at the receiver. For underwater acoustic applications, it is recommended to use a frequency range of 200 to 800 Hz.

*Measuring and estimating Salinity, Conductivity and Density*

Salinity, pressure, temperature, and density are factors that contribute to the conductivity of water. Different levels of salinity have a significant impact on ocean currents. Salinity is typically expressed as a percentage (grams of salt per kilogram of solution). The widely used Practical Salinity Scale (PSS-78) is based on the relationship between salinity and electrolytic conductivity, and it is dimensionless. One formula used to estimate salinity values based on conductivity is:

$$S = 0.008 - 0.1692\, K_{15}^{\frac{1}{2}} + 25.3851\, K_{15} + 14.0941\, K_{15}^{\frac{3}{2}} - 7.0261\, K_{15}^{2} + 2.7081\, K_{15}^{\frac{5}{2}} \quad (49)$$

(E. L. Lewis, 1981)

Conductivity is an important property of water. Pure water itself does not conduct electricity, but dissolved substances like chlorides, sulphates, or carbonates make it conductive. The more dissolved particle in the water, the higher the conductivity. It is worth noting that electromagnetic waves generally penetrate deeper in pure water compared to saltwater.

*CTD Rosette*

The salinity is measured using the CTD (Conductivity, Temperature and Depth) rosette. Additional sensors for important parameters, such as turbidity, oxygen and current meters can also be attached to it.

(Mecklenbräuker, 1998)

The CTD onboard consists of a series of small probes attached to a large metal rosette wheel. The rosette is lowered to the seabed via a cable, and scientists monitor water properties in real-time through a data cable connecting the CTD to a computer on the ship. Using a remote-controlled device, water bottles can be selectively closed during the instrument's ascent. A standard CTD typically takes between two to five hours, depending on water depth, to collect a complete dataset. Water samples are often collected at specific depths to learn about the physical properties of the water column at that particular location and time.

Small, low-power CTD sensors are also used in autonomous instruments:

Water column profilers make repeated measurements of ocean currents and water properties up and down through nearly the entire water column, even in very deep water. These profilers carry basic instruments such as a CTD for temperature and salinity and an ACM (Acoustic Current Meter) for measuring currents, with the capability to add other instruments including bio-optical and chemical sensors.

Spray gliders roam the ocean independently, following pre-programmed routes and occasionally surfacing to transmit collected data and receive new commands. As they traverse horizontally, internal bladders control their buoyancy, enabling them to navigate up and down through the water column akin to whales and other marine creatures.

Floats are floating robots that record profiles or vertical measurement series (e.g., temperature and salinity) in the oceans.

Autonomous Underwater Vehicles (AUVs) are programmable robotic vehicles capable of drifting, driving, or gliding through the ocean without real-time control by human operators, depending on their design. Some AUVs communicate periodically or continuously with operators via satellite signals or acoustic underwater beacons to provide a certain level of control.

Various other accessories and instruments can be included with the CTD package, such as Niskin bottles for collecting water samples at different depths for chemical analysis, Acoustic Doppler Current

Profilers (ADCP) for measuring horizontal velocity, and oxygen sensors for measuring dissolved oxygen content in the water.

Features of CTD sensors include:

- Saltwater resistant
- High accuracy
- Lightweight
- Low power consumption
- Deployable to depths of up to several thousand meters

Note: The small, low-power CTD sensors used on autonomous instruments like water column profilers, spray gliders, floats, and AUVs are more complex to operate. The primary limitation is the need to calibrate individual sensors, especially for autonomous instruments deployed over extended periods. Consequently, sensors must be stable during deployment, or assumptions about seawater properties must be made and referenced to the data. Deep water properties are typically very stable, so autonomous sensor data is matched with historical deep-water properties. STS provides highly precise pressure cells for this specific application.

Compared to the CTD rosette, the hydrophone array has the clear advantage of recording data simultaneously over a longer length (e.g. 130m). The density, salinity, and conductivity can then be estimated through approximation methods, primarily machine or numerical.

### *Hydrometer*

The hydrometer is a measuring instrument for determining the density or specific gravity of liquids.

### *Power density of an antenna and its antenna gain*

The power density of an antenna and its antenna gain are typically measured using specialized measurement instruments and testing procedures:

- **Measuring Power Density:** Power density is typically assessed using a power meter or a spectrum analyser. These instruments can quantify the power of an electromagnetic signal in relation to space and frequency, with the unit of power density being expressed in watts per square meter ($W/m^2$).
- **Measuring Antenna Gain:** Antenna gain is determined using an antenna testing chamber and specialized measurement equipment. This involves characterizing the antenna's directional pattern and calculating its gain. Gain represents the ratio of radiated power to the power radiated compared to an ideal isotropic spherical antenna.

  **Utilizing a Reference Antenna:** To measure antenna gain, a reference antenna with well-established characteristics is often employed. The antenna under examination and the reference antenna are positioned within a test setup, and signal comparisons provide valuable insights into antenna gain.

- **Simulation and Calculation:** In some instances, antenna gain can also be determined through theoretical simulations and calculations based on the physical properties of the antenna. Specialized electromagnetic simulation software tools are commonly utilized for this purpose.

The choice of method depends on specific requirements and the level of measurement precision desired. In practice, combinations of these methods are frequently employed to ensure accurate and dependable results.

# Measurement setup and Data

## Location setup

The vertical antenna (hydrophone chain) and the source were positioned at 5.8 km from each other north of the island of Elba. The static source was securely anchored to the seafloor using ballast. The horizontal displacement (tilt) was within a range of:

$$\pm 200\ m \quad (50)$$

At the source location, the ocean depth is 130m. The vertical antenna used in this setup consisted of N= 48 sensors, spaced equidistantly in 2m intervals, resulting in a total aperture of 94 m. The lowest hydrophone positioned at a depth of -112.7 m, while the highest at a height of -18.7 m. Despite being fixed to the seafloor, the measurement setup still introduced some error due to tilt.

The ocean floor at the measurement site consisted of sand and clay layers. The velocity profile obtained from the CTD rosette (which measured conductivity, temperature, and depth) revealed that the sound velocity was approximately 1525 meters per second up to a depth of about 60 m. Beyond that depth, the sound velocity decreased significantly. The range between 60 m and 80 m may be potentially relevant for this research.

## Data

In the autumn of '93, the [1]NATO SACLANT Undersea Research Centre conducted an acoustic experiment in the Mediterranean. The aim of this endeavour was to obtain acoustic measurement data under highly favourable conditions in a relatively well-charted marine area. Prior to the data collection, a test was conducted against the background noise to estimate the spectrum of observations, revealing a distinctive frequency of 170 Hz above the ambient noise level. This frequency was subsequently selected for transmission. Table 1 presents the key signal-theoretical parameters of the N-Elba experiment. (Mecklenbräuker, 1998).

| Size | Symbol | Value |
|---|---|---|
| **Sensor group** | Hydrophone array vertical | |
| **Sensor distance** | $\lvert r_n - r_{n+1} \rvert$ | 2m |
| **Sensor Nr.** | N | 48 |
| **Source Nr.** | M | 1 |
| **Bandwidth** | F | 150Hz…180Hz |
| **Sampling frequency** | $f_s$ | 1000Hz |

Table 2: Key signal parameters of the N-Elba experiment

## Data Analysis

In the following image, the sensor data from Sensor 20 has been filtered and Fourier-transformed, revealing a clear distinction of the source from the ambient noise. The signal of interest from all sensors is distinctly evident within the frequency range of 50 to 180 Hz. This signal, originating from a source, underwent feedback through a 6-bit shift register with a shift clock frequency of 20 Hz. Subsequently, it was modulated onto a carrier at 170 Hz, and the transmitted bit sequence repeated every 3.15 seconds. The hydrophone data was initially sampled at a frequency of 6 kHz and filtered using a FIR low-pass filter. Since the measurement signal is clearly discernible in each sensor, it can certainly be utilized for analysis.

1 Centre for Maritime Research and Experimentation (STO CMRE)

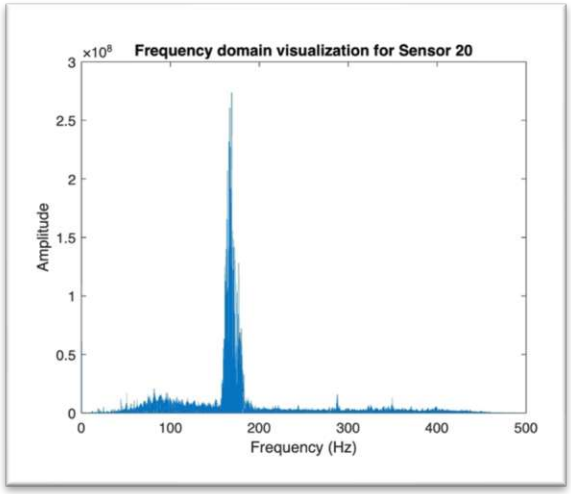


*Figure 11: Frequency domain visualization for Sensor 20: Note the signal of interest at 170 Hz is clearly.*

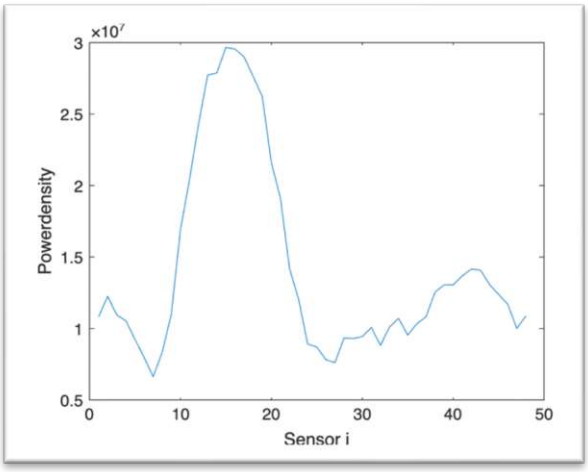


*Figure 12: Power density distribution across all sensors; across the first measurements (half duration of the measurement)*

The power density distribution across sensors is depicted in the Figure 12. Building upon the observation in Figure 11, where the desired signal predominates in amplification compared to other signals, we can infer that the desired signal predominantly contributes to the power density spectrum. In Figure 12, the density remains low up to approximately the first 5 sensors, compared to sensors 6 through approximately 24, after which it decreases again. However, the sound source is positioned at a depth of 65 meters (sensor 24), prompting consideration as to why the power density spectrum is not approximately normally distributed. Several factors contribute to that result:

- Ocean stratification: Oceans are typically divided into layers with variations in temperature, salinity, and density. The near-surface layers, especially the "mixed layer," may be turbulent and efficiently transmit sound waves. Deeper layers may experience higher damping due to lower turbulence or other absorption phenomena, resulting in lower power density.

- Sound propagation effects: Various factors such as temperature, pressure, salinity, and layering influence sound propagation in the ocean. Favorable conditions like lower pressure and higher temperature in the upper layers could enhance sound transmission efficiency, leading to higher power density. Conversely, propagation in deeper layers could be dampened by various factors, resulting in lower power density.

- Reflection and refraction: Sound waves may reflect or refract at boundaries between different layers. Reflections at the water surface or thermocline boundaries in the upper layers could contribute to higher power density. In deeper layers, sound waves may be more heavily damped or behave differently, resulting in lower power density.

- Biological factors: Biological processes such as the presence of phytoplankton or fish can influence sound propagation and power density in the ocean. These biological factors may vary at different depths, contributing to differences in power density.

In comparison, in Figure 13, the higher-level differences are indeed the areas from the 6th sensor downwards to the 24th sensor, which explains the power density spectrum.

The power spectral density plot indicates a significant contrast between sensors 10 to 23, corresponding to the sediment region, and sensors in the oceanic region (approximately sensors 24 to 39). The signal strength is notably amplified at sensor 21 compared to sensor 23, as illustrated in the following figure:

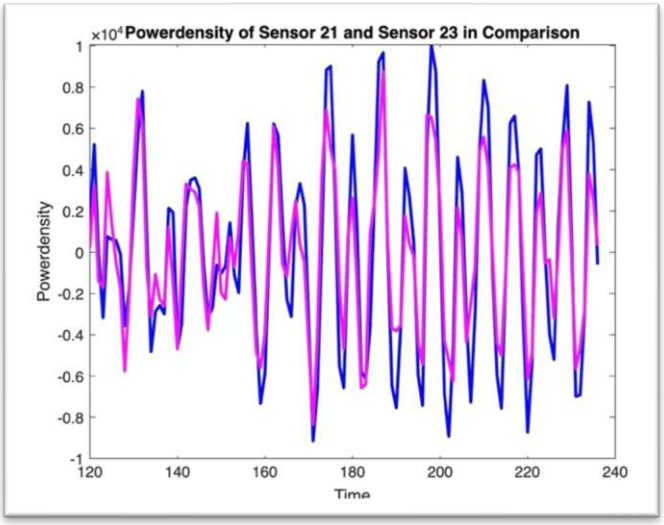


*Figure13: Acoustic pressure recorded over time (120 th measurement till 236 th measurement) by Sensor 21 (blue) and Sensor 23 (magenta).*

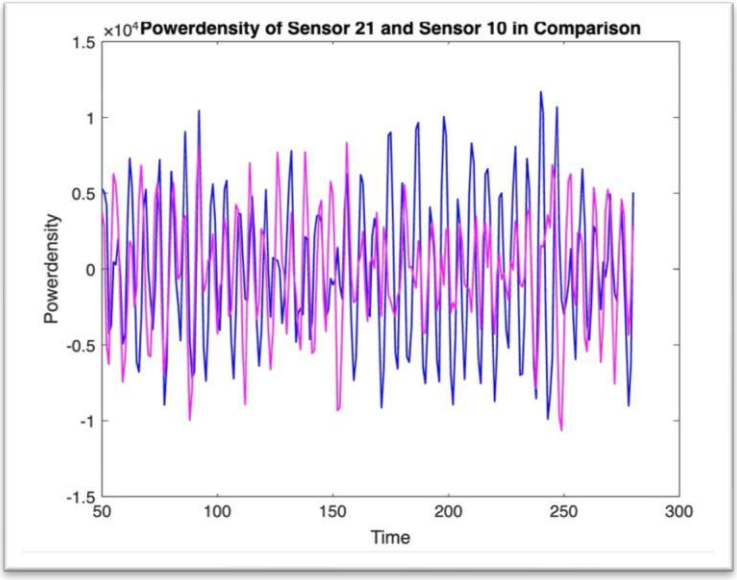


*Figure 14: Acoustic pressure recorded over time (50 th measurement till 280 th measurement) by Sensor 21 (blue) and Sensor 10 (magenta).*

In Figure 14, sensor recordings from Sensor 21 and Sensor 10 were plotted. As known, Sensor 10 arrived attenuated compared to Sensor 21. Additionally, it is evident in the image that the signal arrived with a time delay.

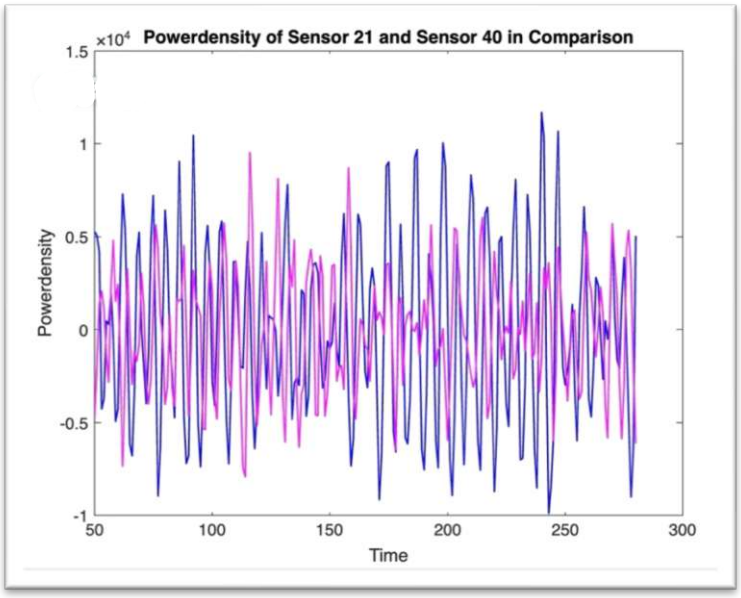


*Figure 15: Acoustic pressure recorded over time (50 th measurement till 280 th measurement) by Sensor 21 (blue) and Sensor 40 (magenta).*

As demonstrated in Figures 13, 14, and 15, high coherence between neighboring sensors is observed, with significant coherence losses evident for sensor 40. Ingo Kalkhoff's diploma thesis emphasizes this observation through the calculation of coherence matrices. Due to the stationary nature of the source during the experiment, coherence and covariance matrices can be computed. He highlights significant coherence losses occurring at sensors 6, 7, 25, and 40. Furthermore, he suggests that these coherence losses may be attributed to variations in propagation velocity during the experiment.(Kalkoff, 1996)

The signal from Sensor 40 appears to have arrived attenuated and time- shifted. Given the stationary nature of the source, a robust covariance matrix of sensor signals can be derived.

Waveforms interfere with each other. Naturally, we perceive them as separate, but due to machine learning, interferences would be incorporated into the final model. To provide a clearer understanding of how the waveforms of the measured data, the initial 500-636 time-discrete values of the 48 sensors were plotted on a heatmap. The resulting visualization distinctly reveals the acoustic wave formation: The 24th sensor is connected reversely, so its data has a 180° phase shift compared to the others.

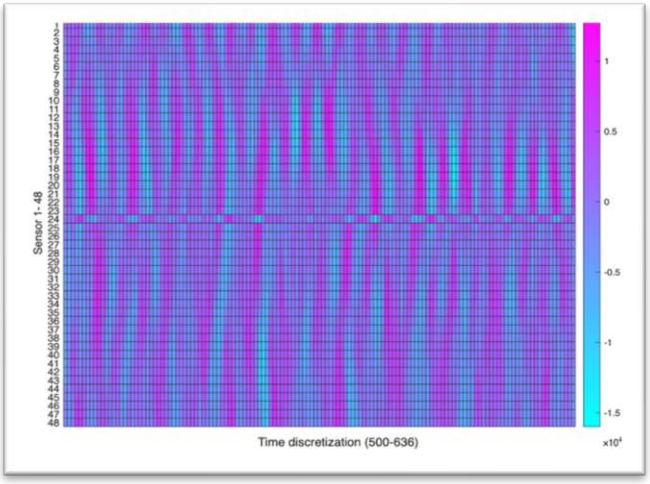


*Figure 21: Heatmap of the acoustic pressure level, of the measured acoustic wave, originated from the source, mentioned in the experiment.*

## Modeling the Measurement Setup

At the specified source location, the water depth measures 130 meters. The seafloor composition at the measurement site was characterized by alternating layers of sand and clay. Notably, data obtained from the CTD rosette, measuring conductivity, temperature, and depth, disclosed that sound velocity exhibited a steady rise, reaching an approximate 1525 m/s up to a depth of about 60 meters. However, beyond this threshold, a marked decline in sound velocity was observed. This intriguing setup lays the foundation for an intricate simulation environment.

### Sound Pressure Field analyzed with Finite Element Method

In the pursuit of acoustic propagation insights, initial results are obtained with a commercially available three-dimensional finite element solver; an isotropic point source emitting a sinusoidal spherical wave at a frequency of 170Hz. The expansive modeling domain spans dimensions of 700 meters in length, 100 meters in width, and 130 meters in height. With the sediment density at the experiment's location constituted by a blend of sand and clay at depths nearing 100 meters (as reported by Mecklenbräuker, 1998), a density of 1750 kg/m³ is embraced within the model. To optimally simulate the data, the velocity value 1550 m/s was adopted at approximately 100 meters depth. This empirically gathered or estimated data was thoughtfully integrated into the modeling framework. Following is an exposition of the finite element method for the N- Elba Experiment with Sediment ($\alpha = 0.13 dB/\lambda$):

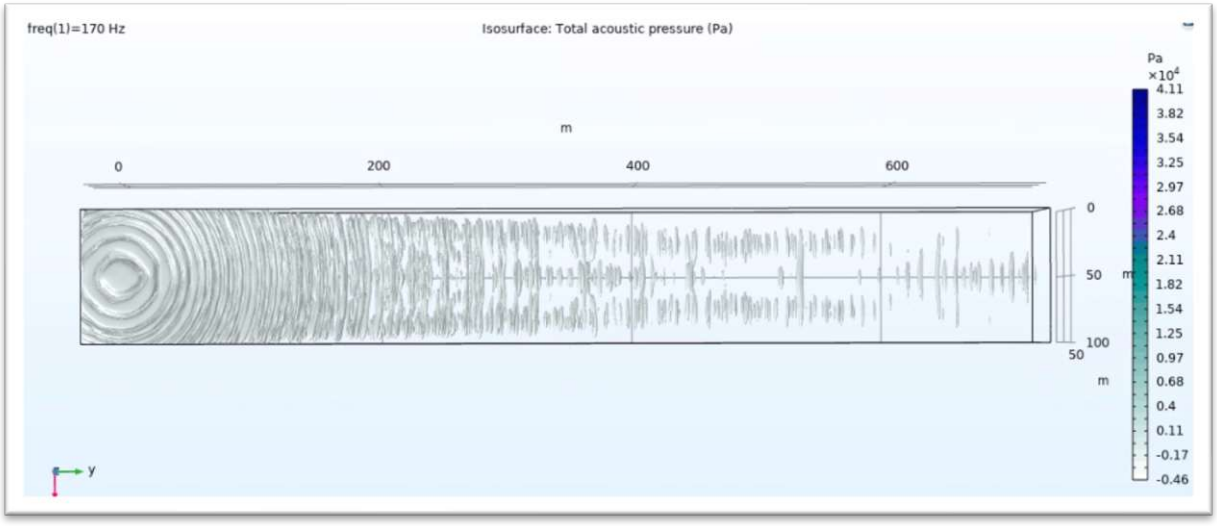


*Figure 16: Sound pressure field Finite Element Method with sediment attenuation, without ocean attenuation; x, y axis*

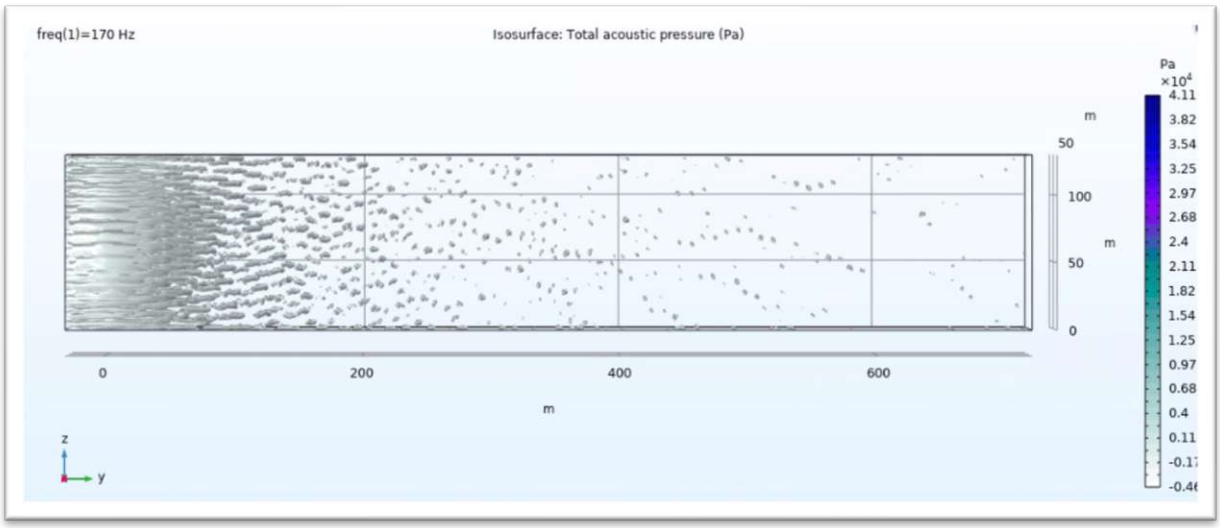


*Figure 17: Sound pressure field Finite Element Method with sediment attenuation; without ocean attenuation; y, z axis*

Another model was generated without sediment to highlight the disparities in the acoustic wave field. In the ensuing images, the acoustic pressure field exhibits notable dissimilarities, while density and sound velocity remain 1510 m/s (Mecklenbräuker, 1998) and 1039 kg/m³ respectively at a depth around 100 meters:

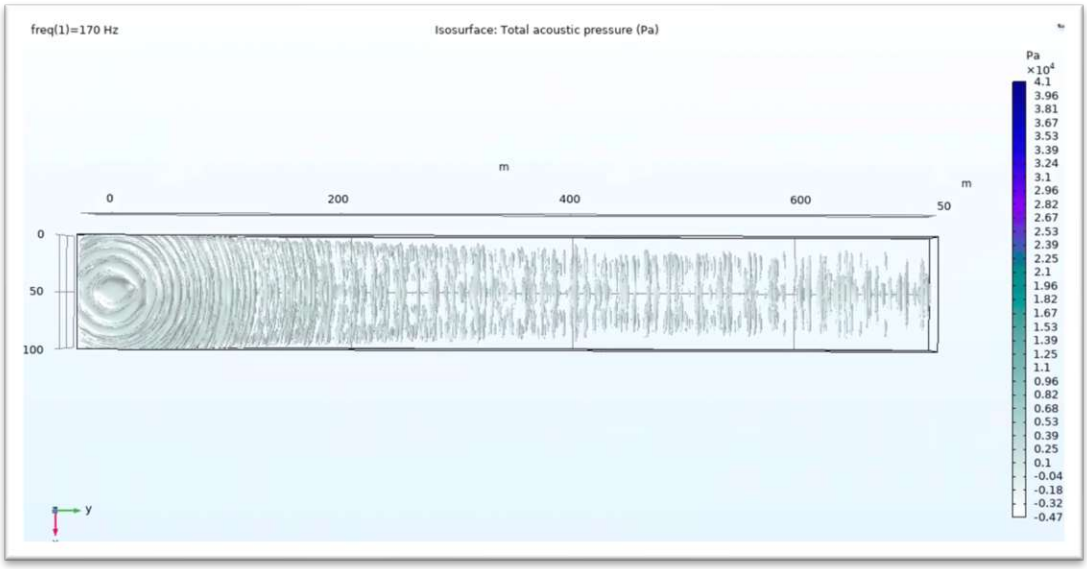


*Figure 18: Sound pressure field Finite Element Method without sediment, with ocean attenuation; x, y axis*

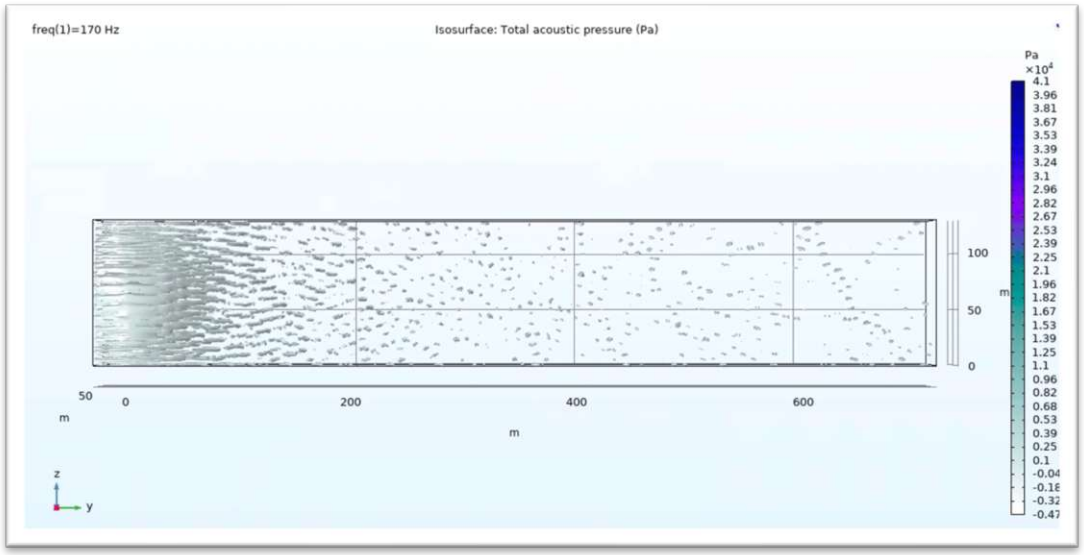


*Figure 19: Sound pressure field Finite Element Method with sediment, with ocean attenuation; y, z axis*

The simulations unequivocally demonstrate that both sediment attenuation and ocean attenuation, including salinity, influence the numerical approximations. It is evident that the addition of sediment to the model significantly attenuates the acoustic pressure field. Through the numerical results (with initial conditions held constant, only varying the damping), it is evident that the acoustic point source is more effectively attenuated when ocean attenuation is considered too. Therefore, it is advisable to consider both models in the analysis of the measurement data.

## Parameter estimation- a machine learning approach

Finite Element Modeling- pressure acoustics analyses were conducted to gather data for a machine-learning model. These analyses revealed variations in the acoustic pressure field corresponding to different propagation parameters. Notably, distinct pressure patterns emerged when accounting for sediment attenuation versus ocean attenuation. Additionally, changes in velocity, such as those observed in the thermocline layer during the N-Elba experiment, were also analysed. However, these velocity changes did not yield significant alterations in the acoustic pressure field. It's worth noting

that analyses into the density of the sediment layer at the bottom were also conducted. It was found that only drastic changes in the density of the sediment layer result in different pressure fields. We can reasonably omit density and velocity for the machine learning model. The carrier frequency of the measured data is 170 Hz.

The proposed study aims to estimate acoustic propagation parameters in shallow oceans using a machine learning approach. Training and testing the model on a dataset comprising recorded, and filtered measurements, with additional information established through physical modeling of the acoustic pressure field (Helmholtz equation). A sketch illustrating the measurement setup and therefore the FEM COMSOL analysis is provided in Figure 20:

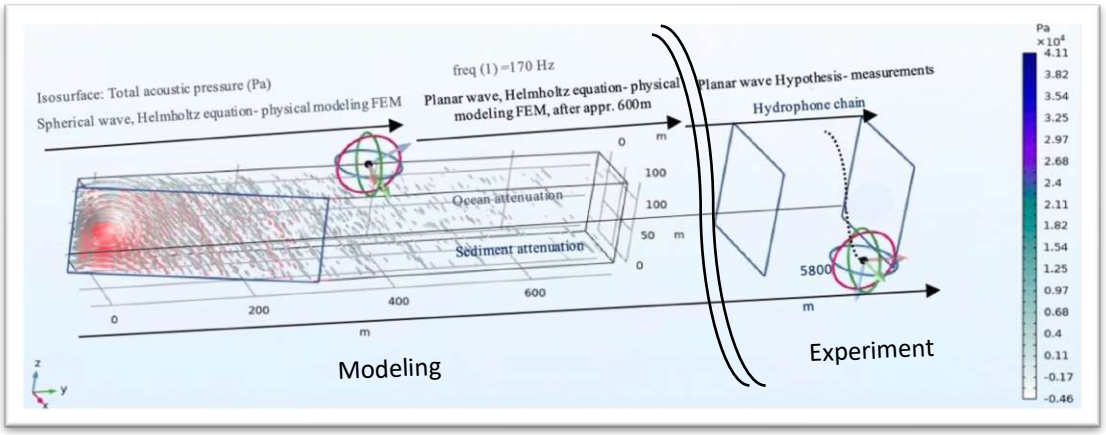


*Figure 20: The sketch demonstrates the modelling in COMSOL of the acoustic pressure field, but also the measurement setup with the hydrophones at the y coordinates: 5800 m; the depth in the measurement setup (as in the COMSOL approximation) is 130 m; the source location in both cases is in the height of approximately 65 m.*

In our exploration of acoustic propagation insights using CTD Data, initial findings for the acoustic pressure fields were obtained through a three-dimensional finite element solver. These models incorporated an isotropic point source emitting a sinusoidal spherical wave at 170 Hz, spanning a domain of 700m x 100m x 130m. The sediment density, composed of sand and clay at depths nearing 100 meters, was characterized with a density of 1750 kg/m³. Empirical data, including a velocity value of 1550 m/s at approximately 100 meters depth, was integrated into the model, providing the foundation for sediment modeling ($\alpha$=0.13dB/$\lambda$).

At the specified source location, with a water depth of 130 meters near the island of Elba, the seafloor comprised alternating layers of sand and clay. Analysis of CTD rosette data revealed a steady rise in sound velocity up to 60 meters, followed by a significant decline. Numerical observations corroborated this pattern, showing minimal changes in the acoustic pressure field in the simulated results, as already mentioned before.

Furthermore, utilizing numerical approximations with FEM COMSOL analysis, we segregated the environment into two distinct layers: ocean attenuation and sediment attenuation. The sensor array group, covering the initial 100 meters of ocean depth (comprising 40 hydrophones), was indicative of ocean attenuation. Conversely, the subsequent 30 meters (encompassing the last 8 sensor values) fell within the range of sediment attenuation. Notably, Figure 21 illustrates higher sound levels in the region characterized by ocean attenuation.

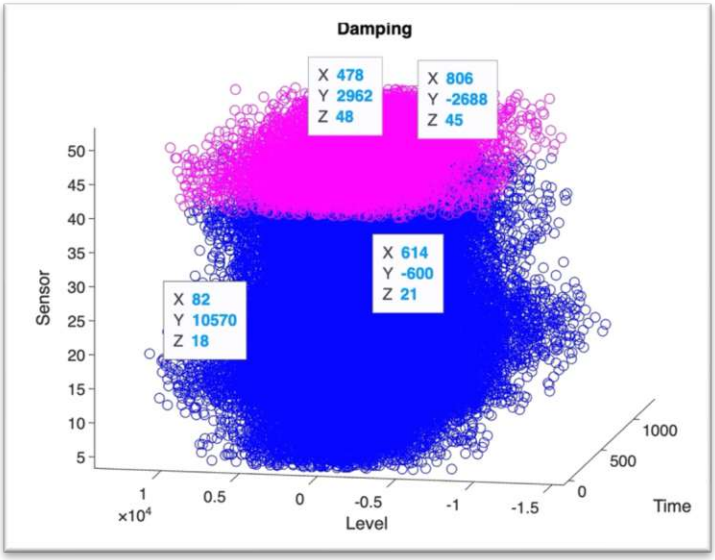


*Figure 21: Damping based on physical FEM model and data measurements that could be affected by the respective damping, sediment attenuation in magenta, ocean attenuation in blue.*

## Related Work

Two distinct methodologies were employed in analysing the N-Elba dataset, each offering unique insights into parameter estimation. In one approach, Bayesian inversion methods were harnessed to derive environmental parameter estimates, accompanied by a comprehensive assessment of the inherent uncertainties in these estimates. The results of this method furnished posteriori probability density functions for the estimated parameters, enabling the extraction of critical information such as means, higher moments, and marginal distributions. (Peter Gerstoft, August 1998) On the other hand, another method featured the development of a generalized likelihood ratio test, which was utilized to test acoustic environmental models and perform parameter inversion using an acoustic propagation code. Notably, both approaches underscored the pivotal role of parameters like source range, source depth, and tilt in shaping the characteristics of the measured data. These investigations shed light on the complex interplay of these parameters within the acoustic environment, offering valuable insights for further environmental characterization. (Mecklenbräuker C. F., 1999)

Traditional methods rely on time-consuming iterative optimization algorithms, leading to potential local optimal solutions. Recognizing the superior performance of neural network algorithms in data processing, the authors of “A Method for Inverting Shallow Sea Acoustic Parameters Based on the Backward Feedback Neural Network Model” propose using a Back Propagation (BP) neural network model as an alternative for inversion purposes. This approach aims to expedite and improve the accuracy of obtaining shallow sea acoustic parameters by replacing traditional iterative optimization methods with neural network models. The paper outlines the methodological approach, emphasizing the establishment of a relationship model between the prediction sound field and the earth sound parameters using a BP neural network. The introduction sets the stage for the subsequent sections which delve into the specifics of the proposed method and its application in retrieving semi-infinite sea bottom sound parameters. (Hanhao Zhu, 2023)

As computer technology advances and power consumption decreases, adopting deep learning algorithms is increasingly recommended for analysing geoacoustic parameters. In this context, exploring a deep learning approach could be beneficial, particularly in addressing regression/ classification problems. There exist several viable methods for this task, including classification, regression, unsupervised learning, and supervised learning techniques. For instance, in scenarios where the objective is to discern between ocean attenuation and sediment attenuation using

measurement data, classification or regression methods may be appropriate. Integrating deep learning methodologies into the analysis offers promising avenues for improving the efficiency and accuracy of parameter estimation in geoacoustic studies.

For the measurements, which involved a single source and receiver setup (although for deep learning approaches, multiple receivers and sources at different locations are typically recommended to train a Neural Network), a series of experiments were conducted employing various methodologies. Ultimately, I opted for a Deep Neural Network- Levenberg-Marquardt Algorithm to analyse the measurements regarding ocean attenuation and sediment attenuation. Alternatives to Levenberg-Marquardt Algorithm optimization algorithm are the Bayesian regularization Algorithm and the scaled conjugate gradient Algorithm.

Following this, a concise list of the techniques and their respective advantages and disadvantages is presented to offer a comprehensive understanding of different approaches in deep learning algorithms. Initially, we address a regression problem for separating sediment from saltwater by using one algorithm from below.

## Machine Learning Algorithms with their respective strengths and weaknesses- an overview

**Levenberg-Marquardt Algorithm**

- Advantages
  - Efficient for nonlinear optimization problems.
  - Lower computational time compared to some other optimization algorithms.
  - Often converges quickly to the minimum.
- Disadvantages
  - Can get stuck in local minima.
  - Sensitive to the choice of initial parameters.
  - Requires a good estimation of the Hessian matrix.

**Bayesian Regularization**

- Advantages
  - Provides a systematic method for addressing overfitting.
  - Accounts for uncertainties in the parameters.
  - Can be effective with small datasets.
- Disadvantages
  - Can be complex and computationally expensive.
  - Requires setting prior and likelihood distributions.
  - May lead to conservative estimates if the prior distribution is not appropriate.

**Scaled Conjugate Gradient**

- Advantages
  - Efficient for large datasets and high dimensions.
  - Does not require computation of matrix Hessians or matrix gradients.
  - Can converge quickly and is relatively robust.
- Disadvantages
  - May perform poorly with very inaccurate initial parameters.
  - Not always as precise as other algorithms like the Levenberg-Marquardt algorithm.
  - May have difficulty in selecting suitable parameters.

It is important to note that the list provides only a brief overview of some of the key techniques in machine learning and may not encompass all possible methods. However, it aims to highlight some significant techniques and their associated strengths and weaknesses.

### Performance of a Machine Learning Algorithm

The performance of a deep learning algorithm can vary greatly depending on factors such as the complexity of the task, the quality and quantity of the data, the architecture of the neural network, the choice of hyperparameters, and the evaluation metric used. There is no fixed range for the performance metric, as it depends on the specific problem being solved.

Common performance metrics for classification tasks include accuracy, precision, recall, F1-score, and area under the receiver operating characteristic curve (AUC-ROC). For regression tasks, metrics such as mean squared error (MSE), mean absolute error (MAE), and R-squared are often used.

- MSE is a metric that indicates the average squared deviation between model predictions and actual data. A lower MSE value suggests that the model predicts the data more accurately and achieves a better fit.
- An R-value typically refers to the correlation coefficient, which measures the strength and direction of the relationship between two variables in a dataset. The correlation coefficient value typically ranges from -1 to 1:
    - A value close to 1 indicates a strong positive linear relationship between the variables, meaning that as one variable increases, the other also tends to increase.
    - A value close to -1 indicates a strong negative linear relationship between the variables, meaning that as one variable increases, the other tends to decrease.
    - A value close to 0 indicates no linear relationship between the variables.

In general, a higher value of accuracy, precision, recall, F1-score, or AUC-ROC indicates better performance for classification tasks, while a lower value of MSE or MAE indicates better performance for regression tasks. However, the acceptable range of performance metrics can vary widely depending on the application and the specific requirements of the problem.

It's important to note that deep learning models often require extensive experimentation and tuning to achieve satisfactory performance, and the performance achieved by a model should be evaluated in comparison to baseline models and domain-specific benchmarks. Additionally, the performance metric should be chosen based on the specific objectives and constraints of the problem at hand.

## Levenberg- Marquardt for Acoustic Propagation Parameters in Shallow Ocean Environments

The Levenberg-Marquardt algorithm is commonly used as an optimization algorithm in nonlinear least squares problems. Independently developed by Kenneth Levenberg and Donald Marquardt, it combines aspects of both the gradient descent method and the Gauss-Newton method. Here are some key points about the Levenberg-Marquardt algorithm:

- **Application**: This algorithm finds frequent application in numerical optimization, particularly in solving nonlinear least squares problems. These may include parameter fitting in curve fitting, regression analysis, or solving inverse problems.
- **Optimization Method**: The Levenberg-Marquardt algorithm merges the gradient descent method with the Gauss-Newton method. It employs an iterative approach to determine optimal parameters that minimize a given objective function.
- **Regularization**: Incorporating a regularization term, the algorithm enhances optimization robustness against poorly conditioned problems. This term ensures that the Hessian matrix

(second derivative of the objective function) doesn't need to be inverted, which can lead to numerical instabilities in poorly conditioned problems.

- **Convergence**: Typically, the Levenberg-Marquardt algorithm converges rapidly, especially near the optimal parameter set. However, convergence heavily depends on the choice of initial values and the characteristics of the objective function.
- **Implementation**: The algorithm necessitates computing the Jacobian matrix (derivative of the objective function with respect to the parameters) and updating the parameters in each iteration. Various implementations and optimizations are available, depending on the specific application, to enhance efficiency.

### Insights of the Levenberg- Marquardt (LM) algorithm

The problem for which the LM algorithm provides a solution is the Nonlinear Least Squares Minimization:

$$f(x) = \frac{1}{2}\sum_{j=1}^{m} r_j^2(x) \quad (51)$$

where $x$ is a vector and $r_j$ is a function from $\mathcal{R}^n \longrightarrow \mathcal{R}$.

The approach combines aspects of Gradient Descent and Gauss-Newton iteration techniques within the Levenberg-Marquardt (LM) algorithm. The update rule employed aims to determine the solution for Least Squares Minimization.

$$x_{i+1} = x_i - (H + \lambda diag[H])^{-1}\nabla f(x_i) \quad (52)$$

where $H$ is the Hessian Matrix evaluated at $x_i$.

### The algorithm

1. Do an update as directed by the equation 52.
2. Evaluate the error at the new parameter vector.
3. If the error has increased as a result to the update, then retract the step (i.e. reset the weights to their previous values) and increase $\lambda$ by a factor of 10 or some such significant factor. Then go to 1. And try an update again.
4. If the error has decreased because of the update, then accept the step (keep the weights at their new values) and decrease $\lambda$ by a factor of 10 or so.

(Ranganathan, 2004).

Overall, the Levenberg-Marquardt algorithm serves as a powerful tool for solving nonlinear optimization problems and finds utility across various applications, particularly in curve fitting, parameter optimization and classification.

### Neural Network Fitting Model for Acoustic Propagation Parameters in Shallow Ocean Environments

The Levenberg-Marquardt (LM) algorithm is commonly utilized with neural networks for predicting output based on input sequences, a prevalent practice in supervised learning tasks such as regression or classification. During training, the LM algorithm iteratively adjusts the neural network's weights and biases to minimize the discrepancy between predicted and actual output values, thereby facilitating learning. Subsequently, the trained neural network is deployed to forecast output values for new input sequences. Post-training, it is customary to validate the network's performance using a separate validation dataset, ensuring its ability to generalize and guarding against overfitting. The effectiveness of predictions depends on factors including data quality, network architecture, hyperparameters, and

the suitability of the LM algorithm for the task. Experimentation and validation play pivotal roles in ensuring prediction reliability. Regression, on the other hand, involves modeling the relationship between a dependent variable and one or more independent variables by fitting an equation to observed data. Neural networks can be employed for regression, offering flexibility in modeling nonlinear relationships and diverse data structures. To utilize neural networks for regression tasks, appropriate network architecture and loss function selection tailored to the specific regression task are crucial. Typically, a simple architecture with a single layer of neurons and a linear activation function is employed, with the mean squared error (MSE) commonly chosen as the loss function for regression, as depicted in figure 22.

*Regression for Acoustic Propagation Parameters in Shallow Ocean Environments*

In the equation 53 $Y$ represents the input, $X$ is the matrix of output variables where rows denote data points and columns represent feature variables, $f(Y)$ describes the relationship between input $Y$ and $X$.

$$X = f(Y) \quad (53)$$

We formulate the problem as a nonlinear least squares problem, aiming to minimize the errors between the observed $X$ and those predicted by $f(Y)$.

In our scenario, each column of the matrix $X$ represents a different time point, and the regression models the relationship between these time points, the corresponding sound pressure level measurements, and the propagation media characteristics.

For the $X$ values, sound pressure level measurements were taken at various discrete time points of equal length (100) intervals, while for the $Y$ values, propagation media characteristics e.g.: damping coefficients, representing ocean attenuation (for the first 40 sensors), and sediment attenuation (for the remaining 8 sensors) and velocity values obtained from the CTD measurements, which were captured simultaneously with the acoustic data, were utilized as the independent input parameters.

Three distinct approaches were implemented:

1. The input data comprised two different attenuation values, ocean attenuation and sediment attenuation.

2. The input data consisted of velocity values obtained from the CTD measurements.

3. The input data included attenuation coefficients and velocity values from the CTD measurements.

These approaches were employed to evaluate the influence of attenuation values, velocity values, and physical modeling using FEM Analysis. As an illustration, we examine Figure 21: the heatmap of the acoustic pressure level, originating from the source mentioned in the experiment, indicates potential sensors possibly situated in the sediment.

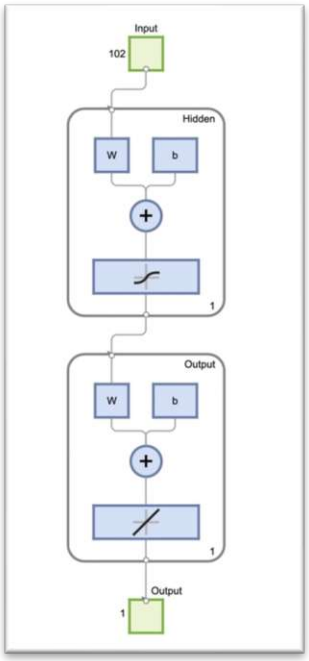


*Figure 22: One layer feedforward network with sigmoid hidden neurons and linear output neurons, suitable for regression tasks*

## Results- Levenberg- Marquardt for Acoustic Propagation Parameters in Shallow Ocean Environments

The neural network depicted in Figure 22 was applied to our independent input variables and output variables, yielding the following results:

The first approach, utilizing input data comprising two distinct attenuation values - ocean attenuation and sediment attenuation, yielded a lower R value compared to the second approach, which relied on velocity values obtained from the CTD measurements. Conversely, the third approach, integrating both attenuation coefficients and velocity values from the CTD measurements, resulted in a lower R value in comparison to the second approach, despite a notable decrease in MSE. The term "R value" likely denotes correlation coefficients, reflecting the strength and direction of the relationship between the input and output data of the model. In this context, the first approach, centred on attenuation values, demonstrates a weaker correlation with the output data compared to the second approach, which emphasizes velocity values. However, the third approach, encompassing both attenuation coefficients and velocity values, exhibits a lower correlation while showcasing a reduction in the mean squared error (MSE), indicative of heightened model accuracy, albeit with a less robust input-output relationship.

## Conclusion- Levenberg- Marquardt for Acoustic Propagation Parameters in Shallow Ocean Environments

The approaches were explored concerning inputs such as ocean attenuation, sediment attenuation, and velocity. The results of the simple machine learning model suggest that the attenuation coefficients exert a greater influence on the model than the simultaneously recorded velocity values. Increasing the complexity by incorporating the source signal (bit sequence) would provide more information and allow for estimating additional parameters. However, detailed knowledge of the acoustic source would need to be included and modeled, thereby increasing the complexity.

## Results- Estimation of electromagnetic conductivity in seawater based on acoustic propagation characteristics

This thesis represents a significant contribution to the exploration of electromagnetic and acoustic wave interactions, particularly pertinent in the context of underwater communication and sensing systems. While acoustic waves are commonly employed due to their efficient propagation characteristics, their susceptibility to interference poses a challenge. Hence, this research endeavors to augment signal accuracy by integrating electromagnetic/optic transmission alongside acoustic waves, thereby mitigating interference issues and enhancing overall system performance.

- Numerical experiments were conducted to investigate the acoustic pressure field for electromagnetic propagation underwater. Analyses revealed that the acoustic pressure field depends more on attenuation (ocean and sediment attenuation) than on velocity. Additionally, numerical experiments showed that changes in electromagnetic conductivity result in variations in penetration depth, particularly under favorable conditions, leading to higher achievable penetration depths.
- The use of simple machine learning models to estimate parameters such as attenuation and velocity based on acoustic data was explored. However, in this case, attenuation and velocity were considered as input parameters, and the sensor level values were considered as output parameters. The results of these simple models suggest that attenuation (both ocean and sediment attenuation) have a stronger influence on sensor level values than velocity values. To estimate additional parameters such as electromagnetic conductivity more comprehensively, it would be necessary to integrate the signal and thus the signal source with its parameters into the models, increasing the complexity level.

The results of this investigation illustrate that both numerical approximations and machine learning models can contribute to providing a comprehensive assessment of various parameters such as attenuation and velocity. Furthermore, by incorporating source information, there is the potential to capture additional parameters such as tilt, density, and temperature. This aspect represents an advancement for future research endeavours as it lays the foundation for precise analysis and interpretation of the underwater environment.

# References

D. F. Gingras, P. G. (1994). *Inversion of geometric and geoacoustic parameters in shallow water: Experimental results.* Saclant Undersea Research Centre.

E. L. Lewis, R. P. (1981). *The Practical Salinity Scale 1978: conversion of existing data.* Pergamon Press.

F.B. Jensen, W. K. (1994). *Computational Oceans Acoustics.* AIP Press.

Hanhao Zhu, Z. C. (23. May 2023). A Method for Inverting Shallow Sea Acoustic Parameters Based on the Backward Feedback Neural Network Model. *Journal of Marine Science and Engineering*.

John L. Butler, C. H. (2016). *Transducers and Arrays for Underwater Sound.* Springer.

Kalkoff, I. (August 1996). Kohärenz in akustischen Wellenfeldern für Sonar bei stochastischen Änderungen des Geschwindigkeitsprofils. *Diplomarbeit*, S. 77.

Koch, C. (1999). *Hydrophone und ihre Kalibrierung für die Messung von Ultraschall.* Braunschweig.

Mecklenbräuker, C. (1998). *Parameterschätzung und Hypothesentests für akustische Wellenfelder unter Berücksichtigung der physikalischen Ausbreitungseigenschaften.* Bochum.

Mecklenbräuker, C. F. (März 1999). Hypothesis testing for geoacoustic enviromental models using likelihood ratio.

Peter Gerstoft, C. F. (August 1998). *Ocean acoustic inversion with estimation of a posteriori probability distributions.* The Journal of the Acoustical Society of America.

Ranganathan, A. (8. June 2004). The Levenberg- Marquardt Algorithm. *academia.edu*.